

# A Novel Combination Scheme for Rayleigh-Taylor Instability Problem in the Laser Ablation Simulation

Cunyun Nie, Haizhuan Yuan, Yuyue Yang, and Shuanggui Li

**Abstract**—The laser ablation is one important part in the inertial confinement fusion (ICF) simulation. The Rayleigh-Taylor (R-T) instability problem is always described as the radiative fluid dynamics equations which are always characteristic of strong nonlinearity and severely discontinuous interface. It can usually be decoupled into radiative fluid dynamics and heat transfer parts with its essential properties. We present a numerical algorithm for the decoupled system. To realize this algorithm, we put forward a combined scheme which inherits some advantages of both FDWENO and RKDG for fluid equations, and construct a symmetric bilinear finite volume element (SBLFVE) scheme for the heat transfer equation. Furthermore, to obtain the proper time step size, we design an adaptive algorithm to harmonize and balance the decoupled system, and to accelerate the computation. We carry on some numerical simulations. Numerical results reveal the bounce phenomena of the shock, the processes of breaking and splitting of thick layer CH, and symmetric temperature distributions, and also show that the reflect wave emerges on some boundary after the laser's erosion. These results also validate the correctness and robustness of the schemes and algorithms.

**Index Terms**—Rayleigh-Taylor instability problem, decoupling algorithm, combined scheme, bilinear finite volume element scheme, adaptive algorithm.

## I. INTRODUCTION

THE radiative fluid dynamics problem, such as inertial confinement fusion simulation, is attractive and challenging for many physics and mathematical researchers all along these years ([1], [2], [3], [4], [5]). To solve the Rayleigh-Taylor instability problem is one important part of inertial confinement fusion experiments, and there appeared many literatures discussing its numerical simulations ([6], [7], [8], [9], [10], [11], [12], [13]). Its characteristics is that the high density fluid with the shape like long spike of rice flows in the low density one, and is that the long spike fluid becomes the shape of mushroom after some periods, and is that the low density fluid is squeezed into the high density region. In ICF numerical experiments, the radiation fluid dynamics problem is described by some control partial differential equations for the laser-driven implosion of a fuel capsule with the goal of igniting a self-sustained reaction. In experiments, the Rayleigh-Taylor instability effects greatly on the inertial fusion, temperature, igniting and flame.

Manuscript received Sept. 22, 2018; revised Feb. 2, 2019. This work was supported by the Project of Scientific Research Fund of Hunan Provincial Education Department (Grant No. 14B044), and the Developing Foundation of CAEP (No. 2015B0202033).

Corresponding author. Cunyun Nie is with the School of Science, Hunan Institute of Engineering, Hunan, 411104, China. e-mail: ncy1028@163.com. Haizhuan Yuan and Yuyue Yang are with the School of Mathematical and Computational Science, Xiangtan University, Hunan, 411105, China.

Shuanggui Li is with the Institute of Applied Physical and Computational Mathematics, Beijing, 10094, China.

In this work, the radiative fluid dynamic problem is decoupled as radiative fluid dynamics and heat transfer parts with preserving its essential properties. Our first work is to design one efficient numerical algorithm for this decoupled system. The first step of it is to obtain a proper guess by solving this system with some explicit scheme. The second step is to renew the temperature and total energy by the state equation. Final step is to obtain the very temperature by solving the energy equation with some implicit scheme. The second work is to present a composite scheme composed of the fifth-order FDWENO and third-order RKDG schemes for fluid equations. It holds the advantages of above two schemes, where the relative function values at fictitious nodes can be provided for each other. We also construct a SBLFVE scheme for the heat transfer equation. The symmetry of it is helpful for numerical simulations. The third work is to put forward a time adaptive algorithm to harmonize the computations between the fluid dynamics and the heat transfer. It can ensure numerical simulation to be accelerative and stable. Numerical simulations are carried on. Numerical results reveal some physical phenomena: the bounce of the stock, the break and split process of thick layer of CH. Numerical results also show that the density has changed after the laser's erosion in the high density region (CH target region), and show that the reflect wave emerges on left boundary at some time, and show that symmetric temperature distributions confirm the heat transfer process. These results validate the correctness and robustness of our novel scheme.

The remainder of this paper is organized as follows. In Section II, we introduce the model problem. In Section III, we present the decoupled algorithm. In Section IV, we design two schemes for the decoupled system. Finally we display numerical results to support our schemes and algorithms.

## II. THE BACKGROUND AND THE MODEL PROBLEM

The radiative fluid dynamics problem usually includes the mass, momentum and energy conservative equations as follows

$$\begin{cases} \frac{\partial \rho}{\partial t} + \nabla \cdot (\rho \vec{u}) = 0, \\ \frac{\partial(\rho \vec{u})}{\partial t} + \nabla \cdot (\rho \vec{u} \vec{u}) + \nabla(P_e + P_i + P_r) = 0, \\ \frac{\partial(\rho E_e)}{\partial t} + \nabla \cdot (\rho E_e \vec{u} + P_e \vec{u}) = \nabla \cdot (K_e \nabla T_e) \\ \quad + \rho W_{ei}(T_i - T_e) + \rho W_{er}(T_r - T_e), \\ \frac{\partial(\rho E_i)}{\partial t} + \nabla \cdot (\rho E_i \vec{u} + P_i \vec{u}) = \nabla \cdot (K_i \nabla T_i) \\ \quad + \rho W_{ei}(T_e - T_i), \\ \frac{\partial(\rho E_r)}{\partial t} + \nabla \cdot (\rho E_r \vec{u} + P_r \vec{u}) = \nabla \cdot (K_r \nabla T_r) \\ \quad + \rho W_{er}(T_e - T_r), \end{cases} \quad (1)$$

where  $T_j, P_j, K_j, E_j$  and  $\varepsilon_j, j = e, i, r$  are the temperature, pressure, heat transfer coefficient, total energy (for unit mass point)

and the ratio of inner energy of the electron, the ion and the photon, respectively, and  $\vec{u}$  is the velocity, and

$$E_j = \varepsilon_j + \frac{1}{2} \vec{u} \cdot \vec{u}, \quad j = e, i, r, \quad (2)$$

and  $\rho$  is the density, and  $W_{ei}, W_{er}$  are the energy exchange coefficients between the electron and the ion, between the electron and the photon, respectively.

In Equation (1), the energy conservation law can be described by three temperature equations from the following relations

$$\varepsilon_j(\rho, T_j) = 1.5\Gamma_j T_j, \quad j = e, i, \quad \varepsilon_r(\rho, T_r) = \frac{1}{\rho} a T_r^4,$$

and there exist some expressions about above physics variables

$$\begin{aligned} K_j &= A_{kj} T_j^{5/2}, \quad j = e, r, \quad K_r = 0.3 \times 10^7 l_r T_r^3, \\ l_r &= A_r \rho^{n_1} T_r^{n_2}, \quad W_{ei} = A_{ei} \rho T_e^{-3/2}, \quad W_{er} = A_{er} \rho T_e^{-1/2}, \\ P_j(\rho, T_j) &= \Gamma_j \rho T_j, \quad j = e, i, \quad P_r(\rho, T_r) = \frac{1}{3} a T_r^4, \end{aligned} \quad (3)$$

and here  $a$  is the size of the target ball, and  $A_{ke}, A_{ki}, A_r, n_1, n_2, A_{ei}, A_{er}, \Gamma_e, \Gamma_i$  are some given constants.

Equations (1) (2) and (3) can constitute a self-closed system for simulating the implosion procession, together with some computation region, initial-value and boundary conditions. To be convenient, we only consider the case of single temperature in one material region. In this case, it can be simplified as the following R-T instability problem

$$U_t + F(U)_x + G(U)_y = f, \quad (x, y) \in \Omega, \quad (4)$$

where

$$\begin{aligned} U &= (\rho, \rho u, \rho v, \rho E)^t, \\ F(U) &= (\rho u, \rho u^2 + p, \rho uv, u(\rho E + p))^t, \\ G(U) &= (\rho v, \rho v^2 + p, \rho vu, v(\rho E + p))^t, \\ f &= (0, 0, 0, \nabla \cdot (K \nabla T) + Q)^t, \\ \rho E &= \rho \epsilon + \frac{1}{2} \rho (u^2 + v^2), \end{aligned}$$

and state equations

$$\begin{aligned} p &= (\gamma - 1) \rho \epsilon, \quad \rho E = \frac{p}{\gamma - 1} + \rho (u^2 + v^2) / 2, \quad p = R \rho T, \\ \epsilon &= C_v T = E - (u^2 + v^2) / 2. \end{aligned}$$

In above equations

$\epsilon$  and  $E$  are the unit volume inner energy and total energy, respectively.

$u$  and  $v$  are the velocity along the direction of x-axis, y-axis, respectively.

$T$  is the temperature, and  $K$  is the heat transfer coefficient

$$\begin{aligned} K &= \begin{pmatrix} k_1 & 0 \\ 0 & k_2 \end{pmatrix}, \quad k_i = a_i T^{5/2}, \quad i = 1, 2, \\ a_1 &= \frac{p}{1 + q T \frac{\partial T}{\partial x} / \rho}, \quad a_2 = \frac{p}{1 + q T \frac{\partial T}{\partial y} / \rho}, \end{aligned}$$

$p$  and  $q$  are some constants.

$Q$  is the heat resource (the laser radiation), and  $R$  is the gas coefficient, and  $C_v$  is the ratio of specific heat.

We will endow equation (4) with some suitable conditions.

(i) Computation region: a rectangle region  $\Omega = \bigcup_{i=1}^3 \Omega_i$  shown as

Fig. 1 where  $\Omega_1, \Omega_2$  and  $\Omega_3$  are the quadrilateral regions ABDC, CDFE and EFHG, respectively.

(ii) Boundary conditions: outflow boundary on  $\Gamma_4$ , wall reflection boundary on  $\Gamma_i, i = 1, 2, 3$ .

(iii) Initial-value conditions: initial density, velocity and temperature at time  $t_0$  are as follows, respectively,

$$\rho_0 = \begin{cases} \rho_1, & (x, y) \in \Omega_1, \\ 1.0 + \delta \cos(250l\pi y/3), & (x, y) \in \Omega_2, \\ \rho_2, & (x, y) \in \Omega_3, \end{cases} \quad (5)$$

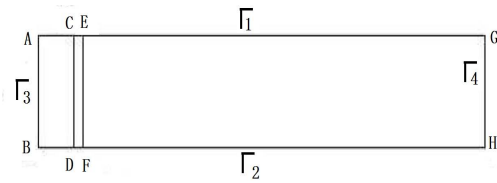


Fig. 1. The computation region.

where  $\rho_1, \rho_2, \delta, l, \pi$  are some given constants,

$$u_0 = v_0 = 0, \quad T_0 = 3.0 \times 10^{-4}.$$

So far, R-T instability problem (4) is well-posed.

### III. DECOUPLING ALGORITHM

Numerical simulations for R-T instability problem (4) are always challenging due to its strong nonlinearity and severely discontinuity. It is usually difficult to solve it directly. Fortunately, it can be decoupled into one radiative fluid dynamics equation and one radiative heat transfer equation as follows

$$U_t + F(U)_x + G(U)_y = 0, \quad (x, y) \in \Omega, \quad (6)$$

$$\rho C_v \frac{\partial T}{\partial t} = \frac{\partial}{\partial x} (K_1 \frac{\partial T}{\partial x}) + \frac{\partial}{\partial y} (K_2 \frac{\partial T}{\partial y}) + Q, \quad (x, y) \in \Omega, \quad (7)$$

where initial and boundary conditions are the same as those before decoupled.

Firstly, we can take the partition for the time interval  $[0, t_e]$

$$0 = t_0 < t_1 < t_2 < \dots < t_N = t_e, \quad (8)$$

and denote  $\Delta t_n = t_{n+1} - t_n, n = 0, \dots, N - 1$ .

Assuming that all variable values at time  $t_n$  are given, we need find those at time  $t_{n+1}$ . We will design some numerical algorithms for Equations (6) and (7) in the following.

#### Algorithm 1:

Step 1: compute the parameters  $a_1, a_2$  at time  $t_n$ , and obtain the variable values  $\rho^{n+1}, u^{n+1}, v^{n+1}, \bar{E}$  at time  $t_{n+1}$  by solving Equation (6), where  $\bar{E}$  is a transition variable.

Step 2: compute  $\bar{T}$  according to the state equation

$$c_v \bar{T} = \bar{E} - ((u^{n+1})^2 + (v^{n+1})^2) / 2.$$

Step 3: obtain the temperature  $T^{n+1}$  at time  $t_{n+1}$  by solving Equation (7) where  $\bar{T}$  and  $\rho^{n+1}$  are treated as the values at time  $t_n$ .

Step 4: compute the new energy  $E^{n+1}$  at time  $t_{n+1}$

$$E^{n+1} = c_v T^{n+1} + ((u^{n+1})^2 + (v^{n+1})^2) / 2.$$

By above 4 steps, we can obtain all variable values at time  $t_{n+1}$ , and finish one time step computation for Equation (4).

#### Remark 1:

(1) In Step 3, we firstly choose a proper time step size  $\Delta t_n$  to solve Equation (6). It will be forced to choose a smaller one and to resolve it if it doesn't converge as solving Equation (7) by using  $\Delta t_n$ .

(2) The Courant Friedrichs condition should be also satisfied with.

(3) The similar algorithm can be employed for other complex system.

### IV. TWO SCHEMES FOR DECOUPLING ALGORITHM

We will introduce a combined scheme for Equation (6) and a SBLFVE scheme for Equation (7), respectively. On the scope of the author's knowledge, there is not any literature on above two schemes composed and employed for the R-T instability problem.

A. The combined scheme

In this subsection, we will display a novel scheme combining the fifth-order FDWENO with third-order RKDG schemes for Equation (6).

We take the quadrilateral partition for Region  $\Omega$ , and denote it as  $\Omega^h = \{E_i, 1 \leq i \leq M\}$ , where  $E_i$  is any element, and  $M$  is the total number of elements. Simultaneously, we take the dual partition of  $\Omega^h$ , and denote it as  $\Omega_k^h = \{b_{X_k}, 1 \leq k \leq N\}$ , where  $X_k = (x_i, y_j)$  is some partition node, and  $N$  is the total number of nodes.

By the backward Euler method, Equation (6) becomes

$$\frac{U^{n+1} - U^n}{\Delta t_n} + F(U^{n+1})_x + G(U^{n+1})_y = 0,$$

where  $\Delta t_n = t_{n+1} - t_n$ . Let  $U = U^{n+1}$ , and we have

$$\frac{U - U^n}{\Delta t_n} + F(U)_x + G(U)_y = 0.$$

The next task is to discretise the term  $(F(U(t, x, y)))_{(i,j)} + (G(U(t, x, y)))_{(i,j)}$  ( Denoted as  $I(t, x_i, y_i)$  ).

The first thing for this task is to discretize  $I(t, x, y)$  by the FDWENO scheme on uniform grids ( $\Delta x, \Delta y$  is the step size along the x-axis and y-axis direction, respectively) at Point  $(x_i, y_j)$  where numerical fluxes should satisfy with the Lipschitz and consistent conditions.

$$I(x, y, t) \approx \frac{1}{\Delta x} (\hat{F}_{i+1/2,j} - \hat{F}_{i-1/2,j}) + \frac{1}{\Delta y} (\hat{G}_{i,j+1/2} - \hat{G}_{i,j-1/2}), \tag{9}$$

where

$$\hat{F}_{i+1/2,j} = \hat{F}_{i+1/2,j}^+ + \hat{F}_{i+1/2,j}^-,$$

$$\hat{F}_{i+1/2,j}^\pm = \sum_{r=0}^{k-1} \omega_r \hat{F}_{i+1/2,j}^{\pm(r)}, \quad \hat{F}_{i-1/2,j}^\pm = \sum_{r=0}^{k-1} \tilde{\omega}_r \hat{F}_{i-1/2,j}^{\pm(r)},$$

$$\omega_r = \frac{\alpha_r}{\sum_{s=0}^{k-1} \alpha_s}, \quad \tilde{\omega}_r = \frac{\tilde{\alpha}_r}{\sum_{s=0}^{k-1} \tilde{\alpha}_s}, \quad \alpha_r = \frac{d_r}{(\varepsilon + \beta_r)^2}, \quad \tilde{\alpha}_r = \frac{\tilde{d}_r}{(\varepsilon + \beta_r)^2},$$

and for the fifth-order FDWENO scheme, we choose  $k = 3$ ,

$$\begin{aligned} \beta_0 &= \frac{13}{12}(U_i - 2U_{i+1} + U_{i+2})^2 + \frac{1}{4}(3U_i - 4U_{i+1} + U_{i+2})^2, \\ \beta_1 &= \frac{13}{12}(U_{i-1} - 2U_i + U_{i+1})^2 + \frac{1}{4}(U_{i-1} - U_{i+1})^2, \\ \beta_2 &= \frac{13}{12}(U_{i-2} - 2U_{i-1} + U_i)^2 + \frac{1}{4}(U_{i-2} - 4U_{i-1} + 3U_i)^2. \\ d_0 &= \frac{3}{10}, \quad d_1 = \frac{3}{5}, \quad d_2 = \frac{1}{10}, \quad \tilde{d}_r = d_{2-r}, \quad r = 0, 1, 2, \end{aligned}$$

and  $\varepsilon = 10^{-6}$  or  $10^{-12}$ ,

$$\hat{F}_{i+1/2,j}^{-(r)} = \sum_{r=0}^{k-1} c_{rj} F_{i-r,j}^-, \quad \hat{F}_{i-1/2,j}^{+(r)} = \sum_{r=0}^{k-1} \tilde{c}_{rj} F_{i-r,j}^+,$$

and  $c_{ij}$  is shown as Tab. 1, and  $\tilde{c}_{rj} = c_{r-1,j}$ ,  $r=0,1,2$ ,

and  $\hat{G}_{i,j+1/2} = \hat{G}_{i,j+1/2}^+ + \hat{G}_{i,j+1/2}^-$  can be similarly presented.

Above choices can helpfully guarantee to solve Equation (6) which inherits both strong discontinuity and great density ratio.

The forgoing thing for this task is to discretize  $F(U)_x + G(U)_y$  by the third-order RKDG scheme on rectangle grids.

For any element  $E_k$  (also denoted by  $E_{i,j}$ ), from the Green formula,

$$\begin{aligned} I(t, x, y) &= \\ &\sum_{e \in \partial E_{i,j}} \int_e (F(U_h(t, \mathbf{x})), G(U_h(t, \mathbf{x}))) \cdot n_{e,E_{i,j}} v_h(\mathbf{x}) d\Gamma \\ &- \int_{E_{i,j}} \left( F(U_h(t, \mathbf{x})) \frac{\partial v_h(\mathbf{x})}{\partial x} + G(U_h(t, \mathbf{x})) \frac{\partial v_h(\mathbf{x})}{\partial y} \right) dx, \end{aligned} \tag{10}$$

TABLE I  
THE COEFFICIENTS  $c_{r,j}$ .

$k$	$r$	$j = 0$	$j = 1$	$j = 2$
1	-1	1		
	0	1		
	1	$\frac{3}{2}$	$-\frac{1}{2}$	
2	-1	$\frac{1}{2}$	$-\frac{1}{2}$	
	0	$\frac{1}{2}$	$\frac{1}{2}$	
	1	$-\frac{1}{2}$	$\frac{3}{2}$	
3	-1	$\frac{11}{6}$	$-\frac{7}{6}$	$\frac{1}{3}$
	0	$\frac{1}{3}$	$-\frac{5}{6}$	$-\frac{1}{6}$
	1	$-\frac{1}{6}$	$\frac{5}{6}$	$\frac{1}{3}$
	2	$\frac{1}{3}$	$-\frac{7}{6}$	$\frac{11}{6}$

where  $\mathbf{x} = (x, y)$ , and  $v_h(\mathbf{x})$  can be usually chosen as some kind of orthogonal basis function  $\phi_{i,j}(x, y)$ , such as

$$\begin{aligned} 1, \quad \alpha_i(x) &= \frac{x - x_j}{\Delta x_h/2}, \quad \beta_j(y) = \frac{y - y_j}{\Delta y_h/2}, \quad \alpha_i(x)\beta_j(y), \\ \alpha_i^2(x) - \frac{1}{3}, \quad \beta_j^2(y) - \frac{1}{3}. \end{aligned}$$

Substituting  $\phi_{i,j}(\mathbf{x})$  into  $v_h$  in (10) and employing Gaussian integral formula,

$$\begin{aligned} I(t, x, y) &\approx \sum_{l=1}^L \omega_l \mathbf{V}_{F,G}^1 \cdot n_{e,E_{i,j}} \phi_{i,j}(\mathbf{x}_{e,l}) |e| \\ &- \sum_{m=1}^M \tilde{\omega}_m \mathbf{V}_{F,G}^2 \cdot \nabla \phi_{i,j}(\mathbf{x}) |E_{i,j}|, \end{aligned}$$

where

$$\mathbf{V}_{F,G}^1 = (F(U_h(t, \mathbf{x}_{e,l})), G(U_h(t, \mathbf{x}_{e,l}))),$$

$$\mathbf{V}_{F,G}^2 = (F(U_h(t, \mathbf{x}_{E_{i,j},m})), G(U_h(t, \mathbf{x}_{E_{i,j},m}))),$$

and

(1)  $\omega_l$  and  $\tilde{\omega}_m$  are the weights,  $\mathbf{x}_{e,1}$  and  $\mathbf{x}_{E_{i,j},m}$  are the Gaussian points on Edge  $e$  and in Element  $E_{i,j}$ , respectively,

(2)  $n_{e,E_{i,j}}$  is the unit outward normal vector, and  $|e|, |E_{i,j}|$  is the length of the edge  $e$ , the area of Element  $E_{i,j}$ , respectively,

(3)  $F(U_h(t, \mathbf{x}_{E_{i,j},m})), G(U_h(t, \mathbf{x}_{E_{i,j},m}))$  can be approximated by some numerical fluxes, such as the Local Lax-Fridrichs splitting.

The final thing for this task is to combine above two schemes. The values at fictitious nodes for FDWENO scheme can be evaluated by the polynomial in some element from RKDG scheme, and the data of fictitious element for RKDG scheme can be reconstructed by those from the forward time step of FDWENO scheme.

So far, the combined scheme has been designed to solve Equation (6).

B. Bilinear finite volume element scheme

By the backward Euler method, Equation (7) leads to

$$\begin{aligned} \rho C_v T - \Delta t_n \left( \frac{\partial}{\partial x} (K_1 \frac{\partial T}{\partial x}) + \frac{\partial}{\partial y} (K_2 \frac{\partial T}{\partial y}) \right) &= \Delta t_n Q + \rho C_v T^n, \end{aligned} \tag{11}$$

where  $T := T^{n+1} = T(t_{n+1})$ ,  $T^n = T(t_n)$ ,

$K_l = K_l(T)$ ,  $l = 1, 2$ .

According to the ‘‘fixed-coefficient’’ method, we can obtain

$$\begin{aligned} \rho C_v T - \Delta t_n \left( \frac{\partial}{\partial x} (K_1^{(k)} \frac{\partial T}{\partial x}) + \frac{\partial}{\partial y} (K_2^{(k)} \frac{\partial T}{\partial y}) \right) &= \Delta t_n Q + \rho C_v T^n, \end{aligned} \tag{12}$$

where  $T := T^{(k+1)}(t_{n+1})$  and  $T^{(k)} = T^{(k)}(t_{n+1})$  are the approximations at the current and forward iterative steps, respectively, and  $K_l^{(k)} = K_l(T^{(k)})$ .

We will construct a symmetrical bilinear finite volume element scheme for Equation (12) (Seen in [14], [15], [16], [17], [18]).

The finite element space  $V_h$  is introduced as follows

$$V_h = \{u_h \in C(\bar{\Omega}) : u_h|_E = \varphi_{\hat{E}} \circ \psi_E^{-1}, \varphi_{\hat{E}} \in \hat{\mathcal{P}}_{1,1}, E \in \Omega^h, u_h|_{\partial\Omega} = 0\},$$

where  $\hat{\mathcal{P}}_{1,1}$  is the set of bilinear functions defined on the standard element  $\hat{E}$ , and  $\varphi_{\hat{E}} \circ \psi_E^{-1}$  represents the composite function between  $\varphi_{\hat{E}}(\hat{x}_1, \hat{x}_2)$  and  $\psi_E^{-1}$ , and here  $\psi_E^{-1}$  is the inverse transformation of  $\psi_E$ , and the bilinear transformation is from  $\hat{E}$  to  $E$ .

Integrating (12) on the dual element  $b_{X_i} \in \Omega_*^h$ , we have

$$\int_{b_{X_i}} \rho C_v T dx - \Delta t_n \int_{b_{X_i}} \left( \frac{\partial}{\partial x} (K_1^{(k)} \frac{\partial T}{\partial x}) + \frac{\partial}{\partial y} (K_2^{(k)} \frac{\partial T}{\partial y}) \right) dx = \int_{b_{X_i}} (\Delta t_n Q + \rho C_v T^n) dx.$$

By the Green formula, we can obtain

$$\int_{b_{X_i}} \rho C_v T dx - \Delta t_n \int_{\partial b_{X_i}} \left( K_1^{(k)} \frac{\partial T}{\partial x}, K_2^{(k)} \frac{\partial T}{\partial y} \right) \cdot \mathbf{n} ds = \int_{b_{X_i}} (\Delta t_n Q + \rho C_v T^n) dx, \quad (13)$$

where  $\mathbf{n}$  is the unit outer normal vector.

Approximated  $T$  by  $T_h \in V_h$  in (13), the balance equation leads to

$$\int_{b_{X_i}} \rho C_v T_h dx - \Delta t_n \int_{\partial b_{X_i}} \left( K_1^{(k)} \frac{\partial T_h}{\partial x}, K_2^{(k)} \frac{\partial T_h}{\partial y} \right) \cdot \mathbf{n} ds = \int_{b_{X_i}} (\Delta t_n Q + \rho C_v T_h^n) dx. \quad (14)$$

One can see that

$$T_h = \sum_{k=1}^4 T_{h,k} \phi_k,$$

where  $T_{h,k} = T_h(X_k)$ ,  $1 \leq k \leq 4$ , and  $X_k, \phi_k$  is the node, bilinear Lagrange interpolation basis function on element  $E$ , respectively.

From Equation (14) and above expression of  $T_h$ , one can also obtain the element stiff matrix  $A^E = (a_{ij}^E)_{4 \times 4}$  and element load vector  $f^E = (f_i^E)_{4 \times 1}$ , where

$$a_{ij}^E = \int_{D_i} \rho C_v dx \delta_{ij} - \Delta t_n \int_{\partial D_i} \left( K_1^{(k)} \frac{\partial \phi_j}{\partial x}, K_2^{(k)} \frac{\partial \phi_j}{\partial y} \right) |_O \cdot \mathbf{n} ds, \quad 1 \leq i, j \leq 4,$$

$$f_i^E = \int_{D_i} (\Delta t_n Q + \rho C_v T_h^n) dx, \quad 1 \leq i \leq 4,$$

and here  $\delta_{ij} = \begin{cases} 1, & i = j, \\ 0, & i \neq j, \end{cases}$ , and  $O$  is the center of element  $E$ , and  $D_i$ ,  $1 \leq i \leq 4$  is the sub-control volume about Node  $X_i$ , respectively.

Assembling all element stiff matrices and load vectors, and dealing with boundary conditions, we can obtain a symmetric bilinear finite volume element (SBLFVE) scheme for Equation (7).

### C. Two schemes' harmonization

We have obtained a combined scheme and a SBLFVE scheme for the decoupled system: Equations (6) and (7), respectively. It is important for them to choose a proper and common time step size  $\Delta t_n$ . Firstly, the CFL condition should be satisfied with. Secondly, it is also vital to harmonize and balance two parts' computations (radiative fluid mechanics and radiative heat transfer). In order to reach it, we design an adaptive algorithm as follows.

#### Algorithm 2:

Step 1: compute the inner energy at the current and forward time steps (denoted as  $\epsilon_{(i,j)}$  and  $\epsilon_{(i,j)}^n$ ) for Element  $E_{i,j}$ , respectively.

Step 2: compute the change ratio of the inner energy for all elements

$$r_{(i,j)} = |\epsilon_{(i,j)} - \epsilon_{(i,j)}^n| / \epsilon_{(i,j)},$$

and find the maximum  $r_{max} = \max_{i,j} \{r_{i,j}\}$ .

Step 3: determine the adjusted time step size according to the  $r_{max}$  for some given change ratio  $r$ , such as 0.1, we design the following three cases:

(1) The time step size preserves  $r$  if  $r_{max}$  is close to  $r$ , i.e.  $r/2 \leq r_{max} \leq 2r$ ;

(2) The time step size becomes smaller than  $r$ , such as 0.8 times  $r$ , if  $r_{max}$  is more than  $2r$ ;

(3) The time step size becomes bigger than  $r$ , such as 1.25 times  $r$ , if  $r_{max}$  is less than  $r/2$ .

Step 4: in addition, we need also adjust the time step size according to the convergence of the nonlinear iteration, for some given maximum iteration number  $N_0$  (Usually chosen as 40), if the real nonlinear iteration number  $N > N_0$ , the time step size should become smaller, such as 0.8r.

## V. NUMERICAL EXPERIMENTS

In this section, we take numerical experiments for two types of R-T unstable problems driven by the gravity force and the laser, respectively.

**Example 1** (Seen in [9])  $U = (0, 0, \rho g, \rho g v)^T$ , computation region  $\Omega = [0, 0.25] \times [0, 1]$ . The initial interface is the line  $y = 0.5$ , and the region where  $y > 0.5$  corresponds to the light fluid, other region does the weight one, and the gravitational acceleration  $g$  is along the y-axis direction.

Boundary conditions:

Left and right : wall boundary,

Above:  $\rho = 1, u = v = 0, p = 2.5$ ,

Below:  $\rho = 2, u = v = 0, p = 1$ .

Initial conditions:

weight fluid:  $\rho = 2, u = 0, v = -0.025c \cos(8\pi x), p = 2y + 1$ ,  
light fluid:  $\rho = 1, u = 0, v = -0.025c \cos(8\pi x), p = y + \frac{3}{2}$ ,  
where  $c = \sqrt{\frac{\gamma p}{\rho}}$  is the speed of sound, and  $\gamma = 5/3, g = 1$ .

We carry on some numerical tests for the fifth-order FDWENO scheme and the combined scheme, where the uniform partition for the region  $\Omega$  is  $N_x \times N_y = 60 \times 240$ , and for the combined scheme: Regions  $y < y_0$  and  $y \geq y_0$  are employed by the fifth-order FDWENO, third-order RKDG schemes, respectively. We obtain the results at time  $t = 1.95$  shown as Fig. 2, where the first one is for the fifth-order FDWENO scheme, and others (from the second one to the fourth one) are for the combined scheme with different interfaces  $y_0 = 0.8, y_0 = 0.75, y_0 = 0.6$ , respectively.

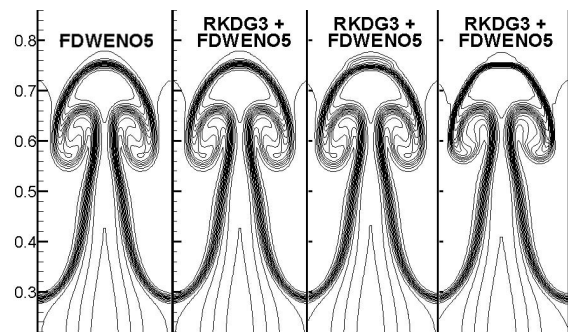


Fig. 2. R-T unstable problem: the fifth-order FDWENO scheme (the first one) and a combined scheme with different interfaces  $y_0 = 0.8, y_0 = 0.75, y_0 = 0.6$  (the second one to the fourth one), respectively.

From above results, one can see that they agree with those in the literature [9] when the interface is far from the discontinuous part, and the accuracy of the results becomes not very well but acceptable. The advantage of this combined scheme is that it can dispose with the composite discontinuous region efficiently.

In the following example, we carry on some numerical tests for the laser-driven Rayleigh-Taylor (R-T) instability problem (4) and realize Algorithms 1 and 2 by two ways: (1) the fifth-order

FDWENO scheme and the SBLFVE scheme, (2) the combined scheme and the SBLFVE scheme, respectively.

**Example 2** For Model problem (4), we choose the parameters as follows.

The computation region  $\Omega$  (unit:  $\mu m$ )

$$AC = 0.1, CE = 0.01, EG = 1, AB = 0.024,$$

and for initial-value conditions

$$\rho_1 = 0.08, \rho_2 = 10^{-3}, \delta = 0.5, l = 1.$$

Some other parameters are as follows

$$R = 57.55, C_v = 86.325, \gamma = 5/3,$$

$$k_1 = a_1 T^{5/2}, k_2 = a_2 T^{5/2},$$

$$a_1 = \frac{p}{1 + qT \frac{\partial T}{\partial x} / \rho}, a_2 = \frac{p}{1 + qT \frac{\partial T}{\partial y} / \rho},$$

$$p = 0.00993957, q = \frac{0.18494 \times 2}{0.3243} \times 10^{-6}.$$

In the region where  $0.1108 \leq x \leq 0.1268$ , the laser radiation resource  $Q$  satisfies with

$$Q = \begin{cases} \frac{3}{16} 10^9 t, & t \leq 0.001, \\ \frac{3}{16} 10^6, & t > 0.001. \end{cases} \quad (15)$$

In this example, we take the uniform partition for Region  $\Omega$ :  $N_x \times N_y = 317 \times 60$ , and the mesh size is  $4 \times 10^{-4}$ . The first and second ways are carried on. Numerical results for the first way are shown as Fig. 3 and Fig. 4, and those for the second way are shown as Fig. 5 and Fig. 6. These results agree with those in the literature [10].

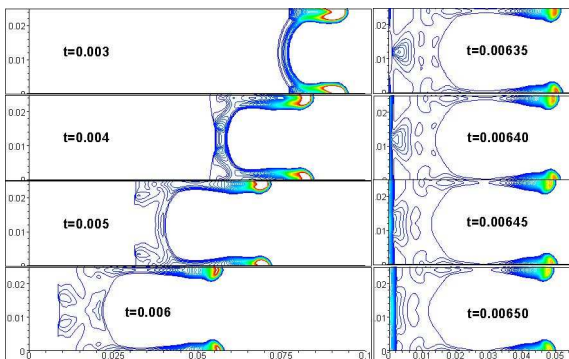


Fig. 3. The density contour for the way (1) FDWENO-SBLFVE scheme.

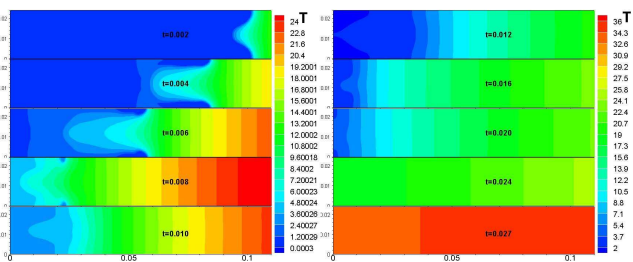


Fig. 4. Temperature distributions for the way (1) FDWENO-SBLFVE scheme.

Fig. 3 shows eight different contours at the corresponding time, respectively. Each of them reports that the bounce phenomena of the stock, the break and split process of thick layer of CH. The density has changed after the laser's erosion in the high density region (CH target region). It also presents that the reflect wave emerges on left boundary at time  $t = 0.0064$ . Fig. 5 shows similar phenomena.

Fig. 4 displays some temperature distributions at different time. It presents good symmetry property, which confirms that the heat transfer is normal. Fig. 6 shows similar phenomena.

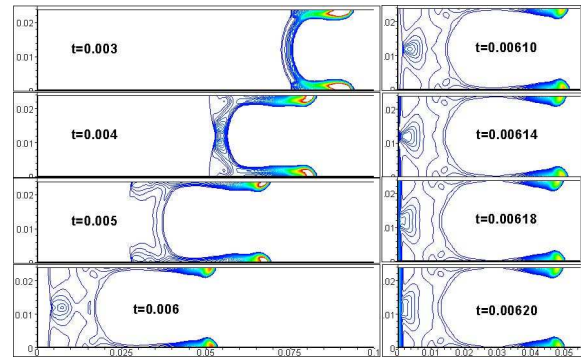


Fig. 5. The density contour for the way (2) combined-SBLFVE scheme.

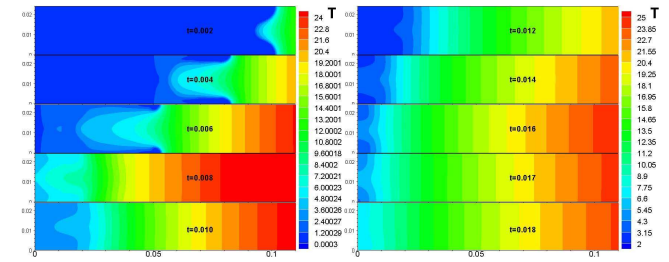


Fig. 6. Temperature distributions for the way (2) combined-SBLFVE scheme.

We can pay attention to the fact that the flexion wave on left boundary makes the convection dominate due to the outmost shell's splitting. It leads to the temperature to become a bit lower locally. However, it increases quickly after that time, and reaches the maximum 36MK at time  $t = 0.027$ .

Numerical results validate the decoupling algorithm and two schemes for the decoupled system. It can provide some references for simulations of ICF problem.

## VI. CONCLUSION

In this paper, the Rayleigh-Taylor instability problem is decoupled into radiative fluid dynamics and heat transfer parts. We put forward a combined scheme which inherits some advantages of both FDWENO and RKDG for fluid equations, and construct a symmetric bilinear finite volume element scheme for the heat transfer equation, and design an adaptive algorithm to harmonize the decoupled system. Numerical results reveal the bounce phenomena of the shock, the processes of breaking and splitting of thick layer CH, the symmetric temperature distributions, and the reflect wave emerging on some boundary after the laser's erosion. These results confirm the validity of the schemes and algorithms.

## ACKNOWLEDGEMENT

The authors thank the referees for their valuable suggestions to improve this paper greatly and are grateful to Professor Shi Shu and Doctor Chunsheng Feng for some helpful discussions on numerical experiments.

## REFERENCES

- [1] P. L. Roe, "Approximate riemann solvers, parameter vectors and difference schemes," *Journal of Computational Physics*, vol. 43, pp357-372, 1981.
- [2] P. D. Lax, X. D. Liu, "Solution of two-dimensional Riemann problems of gas dynamics by positive schemes," *SIAM Journal of Scientific Computing*, vol. 19, no. 2, pp319-340, 1998.
- [3] O. Friedrichs, "Weighted essentially non-oscillatory schemes for the interpolation of mean values on unstructured grids," *Journal of Computational Physics*, vol. 144, pp194-212, 1998.
- [4] Y. Ren, M. Liu, H. A. Zhang, "Characteristic-wise hybrid compact-WENO schemes for solving hyperbolic conservations," *Journal of Computational Physics*, vol. 192, pp365-386, 2005.

- [5] Ch. Yan, J. X. Yu and etc, "On the achievements and prospects for the methods of computational fluid dynamics," *Advances in mechanics*, vol. 41, no. 5, pp562-589, 2011.
- [6] J. Yang, N. Zhao, W. J. Tang, "Fiction fluid methods for nonstable interface numerical simulation," *Chinese Journal of Computational physics*, vol. 20, no. 6, pp549-555, 2003.
- [7] J. Glimm, J. Grove and etc, "The dynamics of bubble growth for Rayleigh-Taylor unstable interface," *Physics of Fluids*, vol. 31, pp447-465, 1988.
- [8] W. H. Ye, W. Y. Zhang, G. G. Chen, "Numerical simulation for the laser Rayleigh-Taylor unstable problem," *High power laser and particle beams*, vol. 10, no. 3, pp403-408, 1998.
- [9] S. Jing, Y. T. Zhang, C. W. Shu, "Resolution of high order WENO schemes for complicated flow structures," *Journal of Computational physics*, vol. 186, pp690-696, 2003.
- [10] S. F. Li, W. H. Ye and etc, "High order FD-WENO scheme for Rayleigh-Taylor unstable problem," *Chinese Journal of Computational physics*, vol. 25, no. 4, pp379-386, 2008.
- [11] J. F. Wu, W. Y. Miao and etc, "Experimental analysis of indirect-drive ablative Rayleigh-Taylor instability on Shenguang II," *High power laser and particle beams*, vol. 27, no. 3, pp1-8, 2015.
- [12] A. N. Kashif, Z. A. Aziz and etc, "Convective heat transfer in the boundary layer flow of a Maxwell fluid over a flat plate using an approximation technique in the presence of pressure gradient," *Engineering Letters*, vol. 26, no. 1, pp14-22, 2017.
- [13] N. Dunna, A. Ramu and D. K. Satpathi, "Numerical solution to strong cylindrical shock wave in the presence of magnetic field," *Proceedings of the World Congress on Engineering 2018*, pp33-38.
- [14] S. Shu, H. Y. Yu, Y. Q. Huang and C. Y. Nie, "A preserving-symmetry finite volume scheme and superconvergence on quadrangle grids," *International Journal of Numerical Analysis and Modeling*, vol. 3, no. 3, pp348-360, 2006.
- [15] C. Y. Nie, S. Shu, H. Y. Yu and J. Wu, "Superconvergence and Asymptotic Expansions for Bilinear Finite Volume Element Approximations," *Numerical Mathematics: Theory, Method and Application*, vol. 6, pp408-423, 2013.
- [16] C. Y. Nie, S. Shu, H. Y. Yu and Y. Y. Yang, "Superconvergence and Asymptotic Expansion for Semidiscrete Bilinear Finite Volume Element Approximation of the Parabolic Problem," *Computer and Mathematics with Applications*, vol. 66, pp91-104, 2013.
- [17] C. Y. Nie, H. Y. Yu, "A Novel Finite Volume Scheme with Geometric Average Method for Radiative Heat Transfer Problems," *Applied Physics Frontier*, vol. 1, no. 4, pp32-44, 2013.
- [18] J. L. Yan and L. H. Zheng, "Linear conservative finite volume element schemes for the gardner equation," *IAENG International Journal of Applied Mathematics*, vol. 48, no. 4, pp434-443, 2018.